IOPscience iopscience.iop.org

Home Search Collections Journals About Contact us My IOPscience

A quantum Monte Carlo method for non-parabolic electron bands in semiconductor heterostructures

This article has been downloaded from IOPscience. Please scroll down to see the full text article.

2005 J. Phys.: Condens. Matter 17 2563

(http://iopscience.iop.org/0953-8984/17/17/004)

View the table of contents for this issue, or go to the journal homepage for more

Download details:
IP Address: 129.252.86.83
The article was downloaded on 27/05/2010 at 20:40

Please note that terms and conditions apply.

INSTITUTE OF PHYSICS PUBLISHING JOURNAL OF PHYSICS: CONDENSED MATTER

J. Phys.: Condens. Matter **17** (2005) 2563–2570 doi:10.1088/0953-8984/17/17/004

A quantum Monte Carlo method for non-parabolic electron bands in semiconductor heterostructures

J Shumway

Department of Physics and Astronomy, Arizona State University, Tempe, AZ 85287, USA

E-mail: john.shumway@asu.edu

Received 23 December 2004, in final form 21 March 2005
Published 15 April 2005
Online at stacks.iop.org/JPhysCM/17/2563

Abstract

We present a many-body computational technique for simulating interacting electrons in non-parabolic semiconductor bands. The technique uses an imaginary time propagator for a non-parabolic electron band that is described by an energy dependent effective mass. This derivation exploits a mathematical analogy between the kinetic energy with effective mass corrected to first order in energy and the relativistic kinetic energy. The propagator can be used in ground state and finite temperature quantum Monte Carlo (QMC) algorithms. We give a demonstration of this path integral QMC technique applied to interacting electrons in a self-assembled InGaAs quantum dot.

1. Introduction

The accurate simulation of electron and hole quasiparticles in semiconductor nanostructures is an important challenge in science and engineering. Two demands, which are often in conflict, are the need to accurately simulate interacting quantum particles and the need to accurately represent the individual quasiparticles [1]. When careful treatment of interactions is important, simplified models such as single-band effective mass models allow the use of analytic techniques [2–4] or quantum Monte Carlo (QMC) simulations [1, 5–8]. When a high quality description of material-specific quasiparticle properties is needed, techniques such as $k \cdot p$ theory [9], empirical pseudopotentials [10], and tight-binding models [11] allow accurate single-particle simulations. To add many-body correlations to these more complicated quasi-particle models, a common approach is a multi-determinant expansion of the few-body wavefunction [12–16]. Such expansions are often underconverged [1], and the multi-determinant techniques scale poorly with the number of quasiparticles.

In this work, we derive a technique for extending the capabilities of quantum Monte Carlo techniques. Band non-parabolicity is often the leading correction to single-band effective mass models of electrons, especially in small bandgap semiconductors [17]. We show that a propagator for electrons with non-parabolic bands can be derived for use in quantum Monte

 © 2005 IOP Publishing Ltd Printed in the UK

Carlo studies. We discuss its application in both ground state and finite temperature QMC algorithms. As a demonstration, we use the techniques to simulate interacting electrons in a self-assembled InGaAs/GaAs quantum dot.

2. Theory: a non-parabolic propagator

In the simplest effective mass formalism, electrons are assigned an effective mass that is the inverse of the second derivative of the energy, $m^* = (\partial^2\varepsilon_k/\partial k^2)^{-1}$, evaluated at the conduction band minimum. For low energy electrons, this single-band approximation is appropriate for many semiconductors. For example, the conduction band in GaAs has a singly degenerate band minimum at the gamma point, with $m^* \approx 0.067m_e$. For higher energy electrons, the non-parabolicity of the conduction band must be taken into account. One way to accomplish this is by treating the electron effective mass as an energy dependent quantity. For example, the conduction band minimum in GaAs is better described by $\varepsilon(k) = \hbar^2k^2/2m^*(\varepsilon)$, where

$$m^*(\varepsilon) = m_0^*(1 + \alpha\varepsilon), \tag{1}$$

where $\alpha \approx 0.6557\,\mathrm{eV}^{-1}$ is the non-parabolicity parameter, and $m_0^* \equiv m^*(0)$ refers to the mass when $\varepsilon = 0$. From the two-band Kane model [17], the energy scale for non-parabolicity is set by the bandgap, E_{gap}, as $\alpha = 1/E_{\mathrm{gap}}$. This expansion can be continued to higher orders in energy. In this paper, we consider only the first-order energy corrections to the effective mass and derive a quantum Monte Carlo technique for the non-parabolic band. Solving for the energy, one finds the standard expression

$$\varepsilon(k) = \frac{1}{2\alpha}\sqrt{1 + \frac{2\alpha\hbar^2k^2}{m_0^*}} - \frac{1}{2\alpha}. \tag{2}$$

This first-order non-parabolic correction is equivalent to fitting the conduction band minimum to a hyperbola, rather than a parabola.

In QMC algorithms, the kinetic energy enters the simulations through the propagator $G(\boldsymbol{r}, \boldsymbol{r}'; \tau) = \langle\boldsymbol{r}|\mathrm{e}^{-\tau H}|\boldsymbol{r}'\rangle$. This propagator is most easily evaluated by expanding in a plane wave basis,

$$\begin{aligned} G(\boldsymbol{r}, \boldsymbol{r}'; \tau) &= \frac{1}{(2\pi)^3}\int \mathrm{d}^3\boldsymbol{k}\, \exp[\mathrm{i}\boldsymbol{k}\cdot(\boldsymbol{r} - \boldsymbol{r}')]\exp[-\tau\varepsilon(|\boldsymbol{k}|)] \\ &= \frac{\exp(\frac{\tau}{2\alpha})}{2\pi^2 r}\int_0^\infty \exp\left[-\frac{\tau}{2\alpha}\left(1 + \frac{2\alpha\hbar^2k^2}{m_0^*}\right)^{1/2}\right]k\sin kr\,\mathrm{d}k, \end{aligned} \tag{3}$$

where $r = |\boldsymbol{r} - \boldsymbol{r}'|$. This integral also occurs in the evaluation of the real-space propagator of a relativistic free particle [18]. In fact, the hyperbolic dispersion relation in equation (2) is mathematically analogous to the kinetic energy of a relativistic particle. In closed form, the propagator is

$$G(\boldsymbol{r}, \boldsymbol{r}'; \tau) = \frac{\exp(\frac{\tau}{2\alpha})\tau}{32\pi^2\alpha z}\left(\frac{2m_0^*}{\hbar^2\alpha}\right)^{3/2}K_2(z), \tag{4}$$

where K_2 is a modified Bessel function of the second kind [19] and

$$z = \frac{\tau}{2\alpha}\left(1 + \frac{2m_0^*\alpha|\boldsymbol{r} - \boldsymbol{r}'|^2}{\hbar^2\tau^2}\right)^{1/2}. \tag{5}$$

When τ becomes large enough, states with small momenta make a dominate contribution to the propagator. In this large τ limit the propagator should coincide with the usual Gaussian propagator for parabolic bands. To verify this limit, expand z for large $\tau \gg m_0^*|\boldsymbol{r} - \boldsymbol{r}'|^2/2\hbar^2\tau$,

$$z \approx \frac{\tau}{2\alpha} + \frac{m_0^*|\boldsymbol{r} - \boldsymbol{r}'|^2}{2\hbar^2\tau}. \tag{6}$$

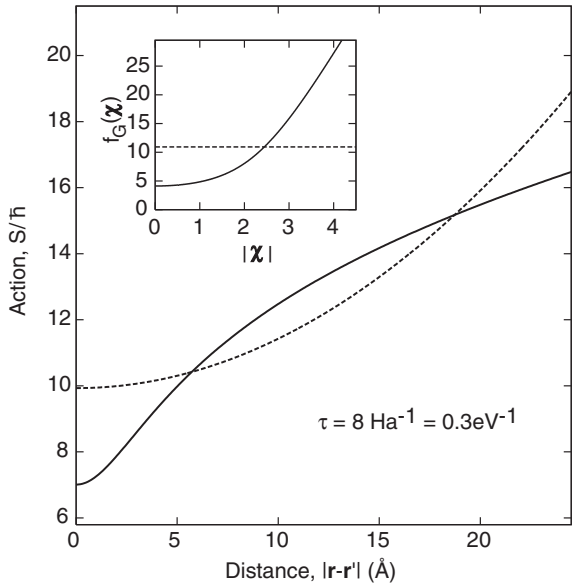

Figure 1. The kinetic action for propagating an electron in GaAs ($m^* = 0.067$) for $\tau = 8$ Ha^{-1} in imaginary time. The solid line includes band non-parabolicity with $\alpha = 0.6557$ eV^{-1}, while the dashed line shows the parabolic action. The inset shows the scale functions for sampling these propagators from a 3D Gaussian variate χ, defined in equation (9).

Using the asymptotic form of the modified Bessel functions, $K_\nu(z) \approx \sqrt{\pi/2z}\exp(-z)$, we find the parabolic band limit,

$$G_0(\boldsymbol{r}, \boldsymbol{r}'; \tau) = \left(\frac{m_0^*}{2\pi\hbar^2\tau}\right)^{3/2} \exp\left(-\frac{m_0^*|\boldsymbol{r}-\boldsymbol{r}'|^2}{2\hbar^2\tau}\right). \tag{7}$$

Note that this limit requires two conditions: the distance $|\boldsymbol{r}-\boldsymbol{r}'|$ must be small enough that $\tau \gg m_0^*|\boldsymbol{r}-\boldsymbol{r}'|^2/2\hbar^2\tau$ is satisfied, and $\tau \gg 2\alpha$.

In figure 1 we compare the parabolic band propagator, G_0, and the hyperbolic band propagator, G. We have plotted the action, $S = -\ln G$, for a time step appropriate for QMC simulations of nanostructures, $\tau = 8$ Ha^{-1} $= 0.3$ eV^{-1}. For the parabolic band propagator, the action is also parabolic, leading to a Gaussian form for G_0. For the hyperbolic band propagator, we see that the action is diminished at both small and large distances. This leads to a propagator, $G(\boldsymbol{r}, \boldsymbol{r}'; \tau)$, that, compared to a Gaussian, has a narrower central peak and longer, exponentially decaying tails. For both the parabolic and hyperbolic bands, the normalization of the propagator is unity, and the root mean square width, $\sigma = \sqrt{\langle|\boldsymbol{r}-\boldsymbol{r}'|^2\rangle}$, is equal to $\hbar\sqrt{\tau/m_0^*}$.

Interactions can be included in the usual Trotter expansion [20]. Writing the Hamiltonian as $\mathcal{H} = \mathcal{T} + \mathcal{V}$, where $\mathcal{T}$ is the kinetic energy operator for non-parabolic bands and $\mathcal{V}$ is the potential energy operator for external confining potentials and for repulsive Coulomb interactions between particles, the Trotter expansion is

$$\exp(-\beta\mathcal{H}) = \lim_{M\to\infty} \sum_M \exp(-\tau\mathcal{T})\exp(-\tau\mathcal{V}), \tag{8}$$

where $\tau = \beta/M$. Explicit use of this formula is known as the primitive approximation [21]. Note that the Trotter expansion naturally introduces non-parabolic effects: if the potential is weak or slowly varying, several sequential kinetic propagators effectively multiply together

to approximate a propagator with a larger effective time step, approaching the parabolic band limit. But if the potential is strong and varies over short times, then the effects of the short time non-parabolic propagators are coupled to the confining potential and are not approximated by the parabolic propagator.

In some cases, such as path integral simulations, we want a more accurate propagator so that we can use a larger time step τ. The action contains free particle terms, $S_0(\boldsymbol{r}, \boldsymbol{r}'; \tau) = -\log G_0(\boldsymbol{r}, \boldsymbol{r}'; \tau)$, and additional terms arising from the potential. In the primitive approximation, the action due to a potential is simply $\tau V(R)$. For pairwise interactions, a useful improvement is the pair approximation [21], obtained from a solution of the interacting two-particle propagator. (Note that, with attractive Coulomb interactions, the Trotter expansion does not hold as written in equation (8), and the pair approximation is needed to maintain a finite time step.) In our simulations, we tabulated the pair Coulomb propagator on a radial grid with a fourth-order polynomial expansion for the off-diagonal coordinate [21], using the analytic expansions of Vieillefosse [22]. We make an additional approximation of using the pair Coulomb density matrix as calculated with parabolic kinetic energy, even when simulating non-parabolic bands. For the external confining potentials we just use the primitive approximation.

3. Simulation technique

Real-space QMC techniques can be used to simulate correlated electrons in semiconductor nanostructures. For ground state simulations, diffusion QMC propagates the electrons along random walks that project out the ground state energy of the system. For finite temperature, path integral QMC samples the quantum partition function represented as a Feynman path integral. We can use this hyperbolic band propagator with both types of QMC algorithms, as discussed in this section.

3.1. Diffusion quantum Monte Carlo

This paper is focused on finite temperature path integral simulations. To introduce a technique for sampling the hyperbolic band propagator, though, the diffusion QMC algorithm without importance sampling is the simplest case. Here we present a brief description of this simple ground state algorithm, and give some references to related calculations for readers who are interested in implementing more practical, importance-sampled ground state algorithms.

In diffusion QMC, the electrons are propagated in a branching random walk [23]. In the simplest formulation, one moves walkers with the free particle propagator, then weights the walkers with a factor $\mathrm{e}^{-\tau V(\boldsymbol{R})}$. To sample the hyperbolic band propagator, one can tabulate a function $f_G(r)$ defined by

$$(2\pi)^{-3/2} \int_0^r \exp\left(-\frac{r^2}{2}\right) 4\pi r^2 \, \mathrm{d}r = \int_0^{f_G(r)} G(r; \tau) 4\pi r^2 \, \mathrm{d}r. \tag{9}$$

From a vector $\boldsymbol{\chi}$ drawn from a Gaussian with unit variance, the vector $\boldsymbol{\Delta r} = \boldsymbol{\chi} f_G(|\boldsymbol{\chi}|)$ samples the hyperbolic band propagator. The function $f_G(r)$ for a typical GaAs simulation is plotted in the inset to figure 1.

The efficiency and stability of diffusion QMC is often improved by importance sampling with a trial wavefunction Ψ_T. With parabolic bands, this leads to a drifted random walk and weighting of walkers based on the trial wavefunction [23]. The hyperbolic band propagator can complicate importance sampling. In this paper, we do not consider importance-sampled diffusion QMC, but instead focus on the path integral QMC method, described next. Some

issues for ground state QMC calculations with this hyperbolic band propagator have been dealt with in relativistic simulations of nuclear models [18, 24, 25].

3.2. Path integral quantum Monte Carlo

The thermal density matrix may be written as a sum over paths,

$$\rho(\boldsymbol{R}, \boldsymbol{R}'; \tau) = \int \mathcal{D}R(t)\ \exp(-S[R(t)]), \tag{10}$$

where the path $\boldsymbol{R}(t)$ starts at $\boldsymbol{R}(0) = \boldsymbol{R}'$ and ends at $\boldsymbol{R}(\beta) = \boldsymbol{R}$. For numerical evaluation, the path is discretized into many short intervals with time step τ, and the action is evaluated for each short interval. Monte Carlo integration may then be used to sample the path integral in order to calculate quantum and thermal averages. For more details of the path integral QMC technique, see the review article by Ceperley [21].

The hyperbolic band propagator makes a contribution to the action,

$$S(\boldsymbol{r}, \boldsymbol{r}'; \tau) = -\frac{\tau}{2\alpha} + \ln(32\pi^2\alpha z/\tau) - \frac{3}{2}\ln\left(\frac{2m^*}{\hbar^2\alpha}\right) - \ln K_2(z). \tag{11}$$

The estimation of energy involves a tau derivative [21],

$$\dot{S}(\boldsymbol{r}, \boldsymbol{r}'; \tau) = -\frac{1}{2\alpha} - \frac{1}{\tau} + \frac{\tau}{2\alpha^2 z^2} + \frac{\tau}{8\alpha^2 z}\frac{K_1(z) + K_3(z)}{K_2(z)}. \tag{12}$$

A key step in the Monte Carlo sampling of a new path configuration is the sampling of a mid-point of a time interval [21]. A common strategy for interacting systems is to use free particle sampling of a new path, with a multilevel rejection scheme for handling interactions [21]. If a free particle is at point $\boldsymbol{r}_{i-1}$ at an earlier imaginary time $-\tau$ and is at a point $\boldsymbol{r}_{i+1}$ at a later imaginary time τ, its current position $\boldsymbol{r}$ has the normalized distribution

$$P(\boldsymbol{r}_i) = G(\boldsymbol{r}_{i+1}, \boldsymbol{r}_i; \tau)G(\boldsymbol{r}_i, \boldsymbol{r}_{i-1}; \tau)/G(\boldsymbol{r}_{i+1}, \boldsymbol{r}_{i-1}; 2\tau). \tag{13}$$

(Recall that the convolution of two Green functions is $G(\boldsymbol{r}_{i+1}, \boldsymbol{r}_{i-1}; 2\tau) = \int G(\boldsymbol{r}_{i+1}, \boldsymbol{r}_i; \tau)G(\boldsymbol{r}_i, \boldsymbol{r}_{i-1}; \tau)\, \mathrm{d}\boldsymbol{r}_i$.) For large times $\tau \gg \alpha$, this is a product of two Gaussians, which is a Gaussian centred between $\boldsymbol{r}_{i-1}$ and $\boldsymbol{r}_{i+1}$. At smaller times, this function is bimodal, with peaks centred around $\boldsymbol{r}_{i-1}$ and $\boldsymbol{r}_{i+1}$.

To sample this joint probability distribution, we use a rejection technique. As an envelope, we sample a point $\boldsymbol{r}_i$ from a normalized sum of two distributions centred around the points $\boldsymbol{r}_{i-1}$ and $\boldsymbol{r}_{i+1}$,

$$P_{2G}(\boldsymbol{r}_i) = [G(\boldsymbol{r}_i, \boldsymbol{r}_{i-1}; \tau) + G(\boldsymbol{r}_i, \boldsymbol{r}_{i+1}; \tau)]/2. \tag{14}$$

The point is accepted with probability $cP(\boldsymbol{r}_i)/P_{2G}(\boldsymbol{r}_i)$, where c is a constant that keeps this probability less than or equal to one at all points. In practice, we find that c can be determined by examining the point $\boldsymbol{r}_i = \boldsymbol{r}_{i-1}$. The rejection rate is very reasonable; typically a third of the points are accepted. In our simulations, we have collected statistics on c and found it to have an average of 0.32 with a sharp peak at a median value of 0.30. Small values of c that would cause many rejections and dramatically slow down the simulation are extremely rare. For example, in a random set of ten thousand values, the smallest value of c was slightly larger than 0.02.

4. Application: path integral simulation of a heteroepitaxial quantum dot

As a demonstration of the technique, we apply it to two electrons in an InGaAs/GaAs self-assembled dot. The non-parabolic effects are significant in this system, and we can nominally compare these calculations to our earlier pseudopotential calculations [26]. A disadvantage of

Table 1. Energies for one and two electrons in an InGaAs dot, in eV, measured from the bulk GaAs valence band edge. Pseudopotential calculations incorporate complete band structure and are used to check our effective mass approximation (EMA) calculations with parabolic ($\alpha = 0$) and non-parabolic ($\alpha > 0$) bands. The total energy of two particles includes small contribution correlations and self-consistent interactions. We can see these small contributions by comparing the total energy (row 4) to the perturbation theory (PT) total energy (row 3). The PT total energy (row 3) for two electrons is twice the single-particle energy (row 1) plus the PT shift (row 2).

			Plane wave EMA		Path integral[a] EMA	
N_e	Quantity	Pseudopotentials[b]	($\alpha = 0$)	($\alpha = E_{gap}^{-1}$)	($\alpha = 0$)	($\alpha = E_{gap}^{-1}$)
1	Total energy	1.420	1.4289	1.4153	1.4293(1)	1.4143(3)
2	PT shift	0.021	0.021	0.023	0.023	0.025
2	PT total	2.861	2.879	2.854	2.8807(2)	2.8536(6)
2	Total energy	—	—	—	2.8800(2)	2.8509(5)

[a] Statistical errors in the last digit of Monte Carlo integrations are shown in parentheses.
[b] Empirical pseudopotential calculation results from [26].

this choice is that the effect of electron–electron interactions are fairly trivial. In these small quantum dots, correlation between two electrons is nearly insignificant relative to first-order perturbative corrections [1]. Correlation does become important in single-dot spectroscopy [1], but inclusion of holes in the calculations introduces other issues that we discuss in the conclusion. Since our focus here is on the improved modelling of electron quasi-particles in QMC simulations, we are content with studying the small-but-calculable effects of band non-parabolicity on the interacting electron energies.

We have used finite temperature path integral QMC simulations for these tests. Taking a low temperature, $T = 0.001$ Ha ≈ 32 K, the system is essentially in its ground state, since the gap to the first excited state is approximately 40 meV [26]. Our motivation for using path integrals for ground state properties is that the algorithm only requires the Hamiltonian: we do not construct trial wavefunctions, but rather sample the density matrix directly. This is useful for nanostructures when we may not know the order of orbital filling or how electrons prefer to distribute themselves in an arrangement of several dots. These simple tests reported here are a necessary step for introducing this hyperbolic band propagator into a larger research project on semiconductor nanostructures [27].

As a test system, we have chosen a model from [26]. In that, a series of quantum dot models with varying size and composition are compared with experimental measurements of size, shape, composition, and photoluminescence spectra. For simplicity, we have chosen one of these model dots: a uniform, conical dot, with the nominal alloy composition of $In_{0.5}Ga_{0.5}As$, having a height of 3.5 nm with a 20 nm base and 16 nm top, and sitting on a 1.85 nm $In_{0.3}Ga_{0.7}As$ wetting layer [26]. As in [26], we have calculated the strained band offsets for electron confinement, using an atomistic valence force field model for the strain calculations [28]. This procedure gives us an effective three-dimensional confining potential to use in our hyperbolic band path integral QMC.

In table 1 we list the energies of one and two electrons from the pseudopotential calculations of [26]. Using a constant effective mass of $m^* = 0.067$ and a plane wave basis, we have checked that energy in the effective mass approximation, as shown in columns 3 and 4 of table 1. (In this study we have kept the mass independent of position for simplicity. As discussed in [29], this approximation is justified because the strain, Ga incorporation, and even the band non-parabolicity effects in the dot all raise the smaller InAs effective mass to a value much closer to that of bulk GaAs. Note in particular that the smaller bandgap in the dot would increase the non-parabolicity factor beyond the constant value that we are using, partially offsetting the

smaller InGaAs effective mass in the dot.) With parabolic bands, the effective mass ground state energy is 1.429 eV, and with non-parabolic bands this energy drops to 1.415 eV.

Next, we ran path integral QMC simulations for one and two electrons in the dot. For one electron, we find that the parabolic and non-parabolic models give very close agreement between the path integral simulation and the plane wave calculation, as summarized in table 1. The plane wave and path integral QMC calculations agree to within 1 meV for both parabolic and non-parabolic bands, giving us confidence in our non-parabolic QMC implementation. In the second row of the table, we show Coulomb energy corrections within first-order perturbation theory, using a dielectric constant $\epsilon = 13$, and corresponding total energies from perturbation theory are shown in the third row. The small differences in absolute values from the perturbative corrections for different methods are probably due to differences in real-space integration techniques. The fact that the pseudopotential Coulomb correction is smaller than the correction obtained with the effective mass may also be due to incomplete convergence of the 'linear combination of bulk bands' basis [30] used with the pseudopotential Hamiltonian [26].

The path integral simulations can directly solve this interacting two-particle system, as shown in the bottom line of the table, using a pair approximation for the Coulomb interactions, as discussed at the end of section 2. The improvements beyond first-order perturbation theory in the path integral calculations for two electrons include both self-consistency corrections and correlation. For the parabolic effective mass calculations, the change is small, about -0.7 ± 0.3 meV. For non-parabolic effective mass calculations, the change is significantly larger, about -2.7 ± 0.8 meV. This is the expected trend: the non-parabolicity softens up the wavefunction, allowing larger self-consistent corrections and more correlation. This is completely analogous to relativistic kinetic energy corrections in atomic physics. The effect can also be understood from perturbation theory: the non-parabolicity significantly lowers the energies of excited states, enhancing higher order perturbative corrections.

5. Conclusion

We have shown a method for including the effects of non-parabolic bands in QMC simulations of semiconductor nanostructures. Tests on a InGaAs quantum dot show that the inclusion of non-parabolicity brings the effective mass calculations into closer agreement with single-electron energies as calculated using empirical pseudopotentials. While this demonstration focused on two electrons, we note that the quantum Monte Carlo formalism can be extended to many electrons with an additional fixed-node approximation [8]. The algorithmic improvements that we have described here should have immediate applications to current QMC simulations of self-assembled dots and enable more realistic simulations of two-dimensional electron gases in real semiconductor heterostructures.

Future work will consider improvement in the simulation of hole states. For strained heterostructures, such as the InGaAs quantum dot considered here, strain breaks the degeneracy of the hole band. These strained holes are sometimes approximated with single-band anisotropic effective masses [2]. In that case, the non-parabolic effects are accompanied by mixing of other hole bands, so the technique described here is not applicable. Rather, techniques that include degrees of freedom for the internal spin and band indices for holes will be necessary to go beyond the parabolic mass approximation for holes.

Acknowledgments

The author thanks Kevin Schmidt for helpful discussions. This work was supported by NSF grant DMR 02-39819.

References

[1] Shumway J, Franceschetti A and Zunger A 2001 *Phys. Rev.* B **63** 155316
[2] Jacak L, Wójs A and Harylack P 1998 *Quantum Dots* (Berlin: Springer)
[3] Yannouleas C and Landman U 2002 *J. Phys.: Condens. Matter* **14** L591
[4] Serra L, Nazmitdinov R G and Puente A 2003 *Phys. Rev.* B **68** 035348
[5] Bolton F 1996 *Phys. Rev.* B **54** 4780
[6] Lee E, Puzder A, Chou M Y, Uzer T and Farrelly D 1998 *Phys. Rev.* B **57** 12281
[7] Harting J, Mülken O and Borrmann P 2000 *Phys. Rev.* B **62** 10207
[8] Shumway J, Fonseca L R C, Leburton J P, Martin R M and Ceperley D M 2000 *Physica* E **8** 260
[9] Bimberg D, Grundman M and Ledentsov N N 1999 *Quantum Dots Heterostructures* (New York: Wiley)
[10] Williamson A J, Wang L W and Zunger A 2000 *Phys. Rev.* B **62** 12963
[11] Lee S, Jönsson L, Wilkins J W, Bryant G W and Klimeck G 2002 *Phys. Rev.* B **63** 235307
[12] Dekel E, Gershoni D, Ehrenfreund E, Spektor D, García J M and Petroff P M 1998 *Phys. Rev. Lett.* **80** 4991
[13] Barenco A and Dupertuis M A 1995 *Phys. Rev.* B **52** 2766
[14] Franceschetti A, Fu H, Wang L W and Zunger A 1999 *Phys. Rev.* B **60** 1819
[15] Williamson A J, Franceschetti A and Zunger A 2001 *Europhys. Lett.* **53** 59
[16] Guffarth F, Heitz R, Schliwa A, Stier O, Geller M, Kapteyn C M A, Sellin R and Bimberg D 2003 *Phys. Rev.* B **67** 235304
[17] Kane E O 1957 *J. Phys. Chem. Solids* **1** 249
[18] Carlson J, Heller L and Tjon J A 1988 *Phys. Rev.* D **37** 744
[19] Abramowitz M and Stegun I 1970 *Handbook of Mathematical Functions* (New York: Dover)
[20] Trotter H F 1959 *Proc. Am. Math. Soc.* **10** 545
[21] Ceperley D M 1995 *Rev. Mod. Phys.* **67** 279
[22] Vieillefosse P 1994 *J. Stat. Phys.* **80** 461
[23] Foulkes W M C, Mitas L, Needs R J and Rajagopal G 2001 *Rev. Mod. Phys.* **73** 33
[24] Carlson J and Pandharipande V R 1991 *Phys. Rev.* D **43** 1652
[25] Carlson J, Pandharipande V R and Schiavilla R 1993 *Phys. Rev.* C **47** 484
[26] Shumway J, Williamson A J, Zunger A, Passaseo A, DeGiorgi M, Cingolani R, Catalano M and Crozier P 2001 *Phys. Rev.* B **64** 125302
[27] Harowitz M, Shin D and Shumway J 2005 *J. Low Temp. Phys.* at press
[28] Martin R M 1970 *Phys. Rev.* B **1** 4005
[29] Wójs A, Hawrylak P, Fafard S and Jacak L 1996 *Phys. Rev.* B **54** 5604
[30] Wang L W and Zunger A 1999 *Phys. Rev.* B **59** 15806